Approaching electrical tomography

Pietro L. Cosentino
Dipartimento di Chimica e Fisica della Terra ed Applicazioni, Università di Palermo, Italy

Abstract
A general approach to electrical tomography is here described, based on the distribution of the experimental data to the set of voxels in which the subsoil has been divided. This approach utilizes the sensitivity coefficients as factors of the convolution procedure to execute the back projection of the data, to obtain the 3D pictures of the subsoil. A subsequent probabilistic filtering technique is described to improve the pictures in view of sharp boundary models. Some models are finally presented, mostly regarding cubic buried anomalies as well as pipe-shaped and *L*-shaped anomalies.

Key words *electrical tomography – electrode grid – back projection*

1. Introduction

The tomographic approach, that is a more or less detailed reconstruction of 2D and 3D images obtained by recovering the space behavior of a physical parameter along a set of pixels (2D) or voxels (3D), has been increasingly used in Geophysics, especially for shallow targets. The methodologies are mainly based on the application of waves or potential fields.

Wave-fields (mechanical or electromagnetic) *tomography* is largely used to investigate the inside of objects also in other technical and scientific fields, like medicine, and is divided into three different classes depending on the main type of waves:

– Transparency or transmission (or refraction) tomography observes the waves propagating from one side to another of the investigated sample.

– Reflection tomography when the study concerns the waves which are reflected by internal discontinuities surfaces of the sample.

– Head-wave (or critical-refraction) tomography, based on the propagation of critically refracted waves along higher velocity layers.

– Diffraction tomography, using one or more sources (in this case coherent sources), analyzes the pattern of diffracted waves.

These techniques work quite well using different frequencies (and correspondingly wavelength) in order to select an appropriate resolution power. They generally observe only kinematic properties of the travelling waves, as the dynamic parameters of the waves (damping, dispersion, etc.) are difficult to study using a single-channel instrument; moreover, the study of dynamic properties on the waves imposes very hard constraints on the technical properties of transducers used by multi-channel instruments.

The principle of *potential-field tomography* is based on the application of a potential field to the sample to be investigated and on the study of the «response» of the sample, *e.g.* the potential field at one point of its external surface. In principle, this response in turn will depend on those of all 3D elementary voxels, which compose the investigated sample.

Mailing address: Prof. Pietro L. Cosentino, Dipartimento di Chimica e Fisica della Terra ed Applicazioni, Università di Palermo, Via Archirafi 26, 90123 Palermo, Italy; e-mail: pietro.cosentino@unipa.it

When the potential field used is artificial and/or the sample to be studied can be differently oriented, the field can be generally applied to the sample in a lot of different ways; in all cases, however, the responses can be observed in every point of the external surface, giving a set of pieces of information which have to be suitably integrated to obtain the tomographic «imaging».

While in some wave-field tomographies (*e.g.*, reflection tomography) the information is directly related to particular internal «surfaces» of the sample, using potential-field tomography the information is related to the various «volumes» which contribute to the response.

The main potential-fields used for tomographic geophysical investigations are electric, magnetic and gravimetric fields. The electric one is generally much more powerful and flexible than others due to the large possibility of different ways to energize the sample (direction, size and shape of the field sources, etc.): most of them are easy to apply for most of the sample to be investigated.

Therefore electric tomography can be performed by:

i) A multiple (sometime also single) application of an electric field to the sample to be investigated.

ii) Measurements of the electrical field (or potential difference, or apparent resistivity) in a set of selected points on the external surface (or also inside) the investigated sample.

iii) The solution of the «inverse problem», that is retrieving a resistivity model, which should be carried out starting from a simple «fragmented» body, made up of elementary 3D or 2½D cells (called voxels, VOlume piXELS).

The inverse problem can sometimes be solved by means of a simple «back-projection» of the experimental data, leading to interpretative models sometimes very useful as preliminary «images» of the «final» model. The advantages of this kind of technique with respect to the classical «inversion» of the data are:

i) It does not require any *a priori* interpretative model other than a fragmentation of the sample in a number of elementary voxels: the only subjective choices are the size of the voxels and matching the grid with the sample (Cosentino and Luzio, 1997).

ii) The resolution, which drives the choice of the voxel size, is directly linked only to the quality and quantity of experimental data thereby avoiding large equivalence limits.

iii) It is very cheap in terms of computer time.

On the other hand, the main disadvantage is that it does not recover the actual resistivity of the structures but only the «shadows» of resistive and conductive voxels (or groups of voxels) without any clear connection with the values (the equivalence is much larger than that associated with inversion procedures). In other terms, it represents the geometry of the structures but not their actual resistivity values.

This kind of approach has a further, sometime very interesting, advantage with respect to the inversion methods as well as other tomographic approaches: the apparent-resistivity measurements carried out by means of different (both in type and size) electrode arrays can be used all together to obtain the back-projected resistivity voxels of the subsoil. The integration does not disturb the back projection process; on the contrary, it gives some additional information to investigate in more detail some parts of the subsoil.

2. A general tomographic approach

Let us describe the subsoil using a model, which is discretized in many elementary cells (3D voxels, fig. 1). The «anomalous» resistivity of a voxel can modify an experimental resistivity measurement (apparent resistivity) carried out using a general four-electrode array. The influence factors of all the voxels have been first calculated on the basis of the anomaly of apparent resistivity due to an elementary resistive sphere centered on the pixel center (Cosentino *et al.*, 1995). Subsequently, due to a practical coincidence of the obtained values, these factors were calculated (Cosentino *et al.*, 1997) in a discrete set of representative points of a homogeneous ground, by means of the formulas given for the influence of the elementary volumes («sensitivity», after Roy and Apparao, 1971).

The influence density function of a generic «point» (x, y, z) of the subsoil on a resistivity

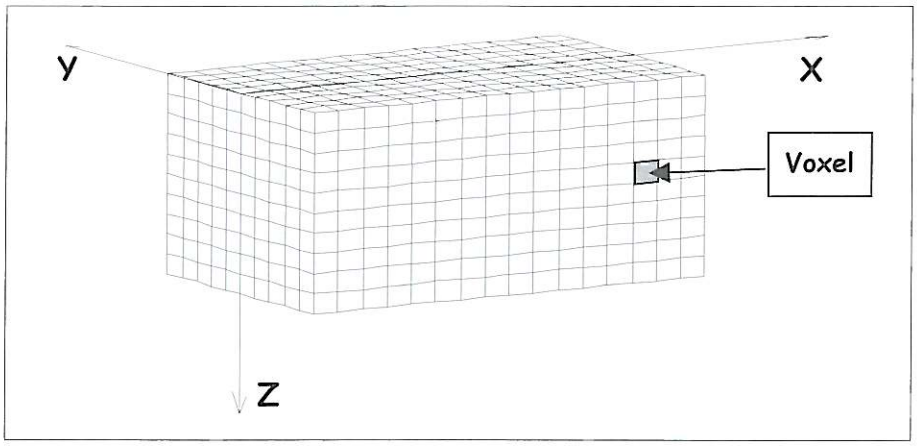

Fig. 1. The model of the subsoil is discretized in a set of cubic voxels.

measure carried out with a four electrode linear array can be expressed as:

$$
\begin{aligned}
I(x,y,z) = {} & [\xi_{11}+\eta_{11}+z^2]\{[(x-x_{C1})^2+ \\
& (y-y_{C1})^2+z^2][(x-x_{P1})^2+(y-y_{P1})^2+z^2]\}^{-3/2}+ \\
& -[\xi_{21}+\eta_{21}+z^2]\{[(x-x_{C2})^2+ \\
& (y-y_{C2})^2+z^2][(x-x_{P1})^2+(y-y_{P1})^2+z^2]\}^{-3/2}+ \\
& -[\xi_{12}+\eta_{12}+z^2]\{[(x-x_{C1})^2+ \\
& (y-y_{C1})^2+z^2][(x-x_{P2})^2+(y-y_{P2})^2+z^2]\}^{-3/2}+ \\
& +[\xi_{22}+\eta_{22}+z^2]\{[(x-x_{C2})^2+ \\
& (y-y_{C2})^2+z^2][(x-x_{P2})^2+(y-y_{P2})^2+z^2]\}^{-3/2}
\end{aligned}
\tag{2.1}
$$

where $\xi_{ij} = (x-x_{Ci})(x-x_{Pj})$ and $\eta_{ij} = (y-y_{Ci})(y-y_{Pj})$. The coordinates of the current electrodes are $(x_{C1}, y_{C1}, 0)$ and $(x_{C2}, y_{C2}, 0)$ while those of the potential electrodes are $(x_{P1}, y_{P1}, 0)$ and $(x_{P2}, y_{P2}, 0)$.

To find the influence of a finite volume (voxel), the integral of the function (2.1) has to be extended to the whole volume of the voxel. But this integration for some voxels is rather critical due the high-gradient values of the function and the relatively large size of the voxel edge (furthermore relation (2.1) unfortunately diverges just in the points where the electrodes are located). To reduce the problems, the voxel size should be selected as small as possible for function (2.1) to be quite constant within that volume. The target is, however, a compromise: smaller voxels give high flexibility to the models and need a large amount of experimental data to reach the desired detail of information, but they also involve a higher number of voxels, which in turn require larger computer memory and are time-consuming to process in the subsequent back-projection.

An interesting coefficient, the Partition Level (PL) can be defined as the ratio between the smallest distance between two electrodes of the array and the selected size of the pixels. The PL value characterizes the approximation errors as well as the resolving power of the subsequent back-projection.

Some examples of the space behavior of the influence coefficients are presented: in fig. 2 the coefficients along a section parallel to and slightly apart from the line of a Pole-Pole array and in fig. 3 those calculated for the same section with respect to a Pole-Dipole array, having respectively a dipole order n = 4, 5 and 6.

It should be noted that there are both positive and negative coefficients: the physical meaning

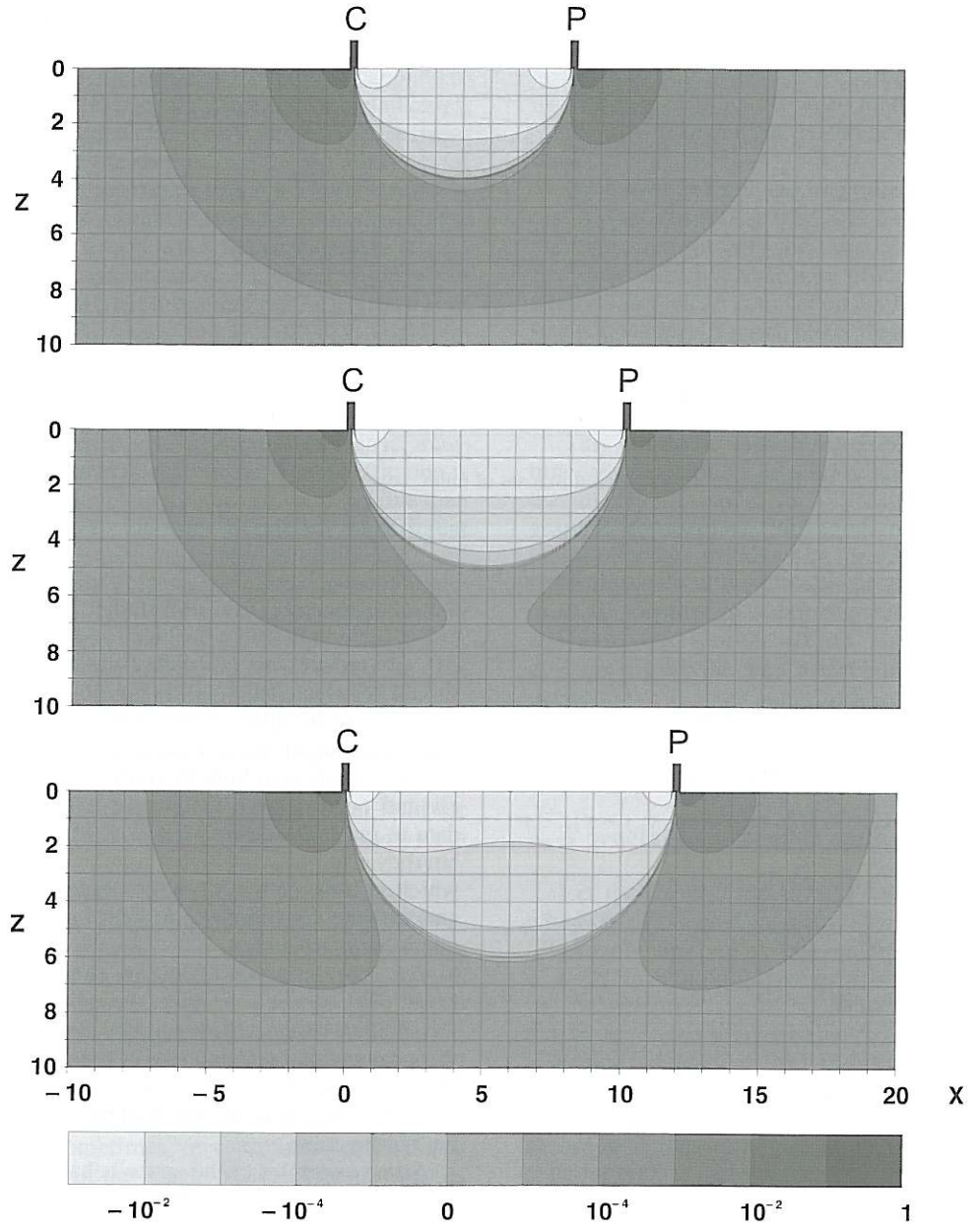

Fig. 2. Influence factors of the voxels of a vertical section slightly apart from the line of the electrodes ($y = 0.5$) on a single apparent resistivity measure carried out using pole-pole array. The influence coefficients are represented for three different values of the partition level, namely PL = 8 (top); PL = 10 (medium), and PL = 12 (bottom). Positive values of the influence factors are located in the external parts, while negative influence factors are located in the inner part (after Cosentino *et al.*, 1998a).

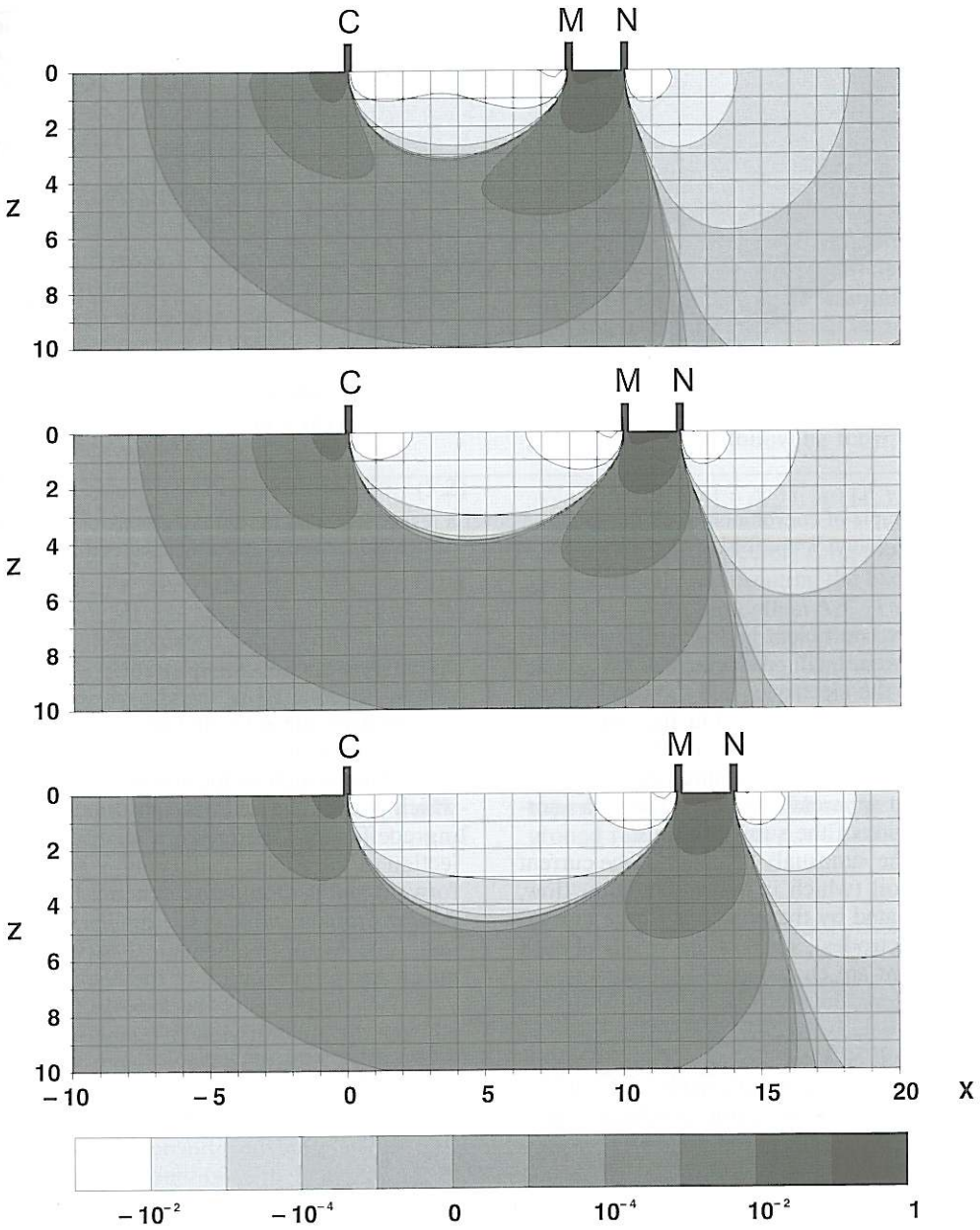

Fig. 3. Influence factors of the voxels of a vertical section ($y = 0.5$) for a single apparent resistivity measure carried out using a pole-dipole array. The influence coefficients are calculated for PL = 2 and three different values of the dipole order, namely $n = 4$ (top), $n = 5$ (medium) and $n = 6$ (bottom). Positive values of the influence factors are located in the external part behind the current electrode and in the inner part between the potential electrodes, while negative influence factors are located between the current and potential electrodes and at the back of the potential electrodes (after Cosentino *et al.*, 1998a).

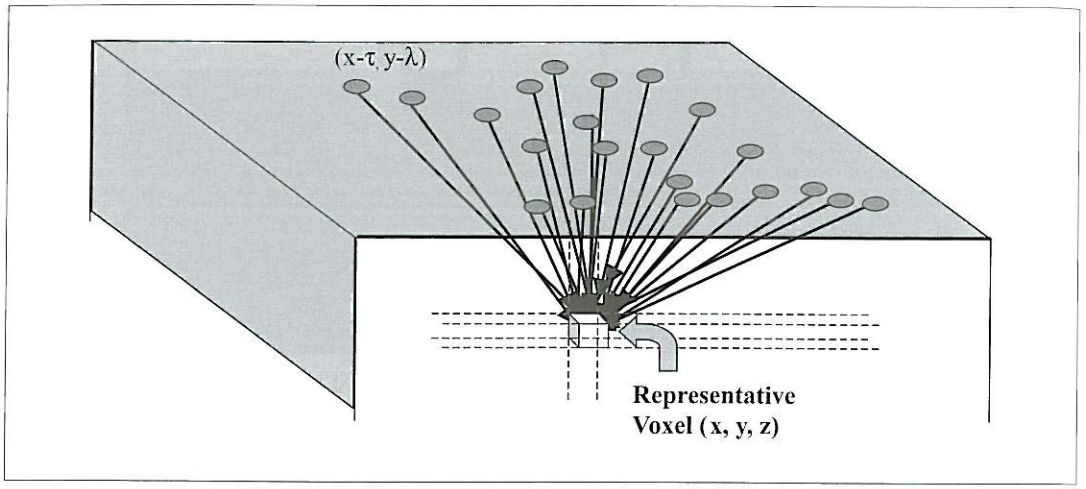

Fig. 4. Example of convolution of all the data to recover a resistivity value for the representative voxel. Each experimental datum is ascribed to a «point» of the surface, which is here represented by a dark circle.

of a positive coefficient is that a more resistive mass in the voxel will produce an increase in the potential at the electrodes and then an increase in the apparent resistivity. On the contrary, a conductive mass in the same voxel will produce a decrease of both the measured potential and the resultant apparent resistivity. This is a «normal» behavior of the subsoil voxels.

Due to the «unusual» behavior of the current in the subsoil (which is not a «laminar» flow, but is regulated by the positions of the current «point»-electrodes), some of the voxels of each measurement are characterized by negative influence factors: the physical meaning of a negative coefficient is that a more resistive mass in the voxel will produce a decrease of the measured potential and then a decrease of the apparent resistivity; therefore a more conductive mass in the same voxel will produce an increase in both the measured potential and the consequent apparent resistivity. However, a possible negative link between a part of the subsoil and a resistivity measurement is well known in resistivity prospecting.

In this methodology, in which the recovery of the behavior of the resistivity in the subsoil is carried out by means of a back projection of all the experimental data, some problems arise due to the difficulty to detect one of the two possible cases: a positive resistive anomaly (larger value of apparent resistivity) can be caused either by a «resistive» mass located in a voxel which is linked by a positive coefficient or by a «conductive» mass which is located in another voxel, which is then characterized by a negative linking coefficient. Therefore, a simple back-projection of the experimental data is not straightforward and it should also account for this important problem, which also implies some problems due to the mathematical aspects of the necessary normalization of the coefficients.

In fact, the process of back-projection, watched from the point of view of a single voxel, can be regarded in such a way: a sort of weighted average should be found among all the resistivity data on which the voxel gave its influence (fig. 4). Therefore the influence coefficients have to be weighted: the presence of positive and negative values is difficult to handle in such a normalization procedure.

3. Back projection of the experimental data

In a set of N experimental data (values of apparent resistivity $\rho_a[x, y]$), the resistivity of a

generic voxel located in the point (x, y, z) should be calculated by such a convolution of all experimental data

$$\rho(x, y, z) = \int\int^{N} g(\tau, \lambda, z)\rho_a[x, y]\, d\tau d\lambda \qquad (3.1)$$

τ and λ being the coordinates of the «centers» of the arrays used to acquire the apparent resistivity data with respect to the selected (infinitesimal) voxel and $g(x-\tau, y-\lambda, z)$ the normalized convolution coefficient linking the selected voxel with all the measured resistivity data. Intervals in τ and λ are extended to all positions of N data.

In practical applications, relation (3.1) becomes

$$\rho(x, y, z) = \sum_{i=1}^{N} f_N(\tau_i, \lambda_i, z)\rho_{a_i}[x, y] \qquad (3.2)$$

where $f_N(\tau_i, \lambda_i, z)$ is the convolution coefficient normalized for the (finite, with size S) voxel (x, y, z) using all data and it is linked to $g(\tau, \lambda, z)$ trough a volume integral.

It should be noted that at the same «point» of the surface two (or more) different experimental data can be connected with a selected voxel with two quite similar influence coefficients (for instance, measured with the same array and different azimuth) or with two different coefficients (due, for instance, to different type of arrays or to different size of the array used for collecting the data): in the latter case the two measurements have to be used as two different unrelated data.

It would be very easy to calculate the coefficients of the g-filter without negative values of influence coefficients, since the normalized values of these coefficients could give a complete set to carry out the convolution. Unfortunately, the presence of negative coefficients (or sensitivities) complicates the assignment of the weights, as they either should be set to zero or should be somehow integrated in the filter.

A useful artifice can be made on the basis of the following assumption. Consider the experimental data in the following form:

$$\rho_a[x, y] = \rho_{a_{ref}} + \Delta\rho_a[x, y] \qquad (3.3)$$

where $\rho_{a_{ref}}$ is a selected reference resistivity value (actually representing the background resistivity, always larger than $\Delta\rho_{a_{max}}$) and $\Delta\rho_a[x, y]$ is the (positive or negative) resistivity anomaly of the datum acquired in the relative position $[\tau, \lambda]$ (fig. 5).

We can invert the negative influence coefficients, when the link between voxel and datum is negative, provided that we «invert» also the experimental anomaly with respect to the background reference value $\rho_{a_{ref}}$. In other words, the

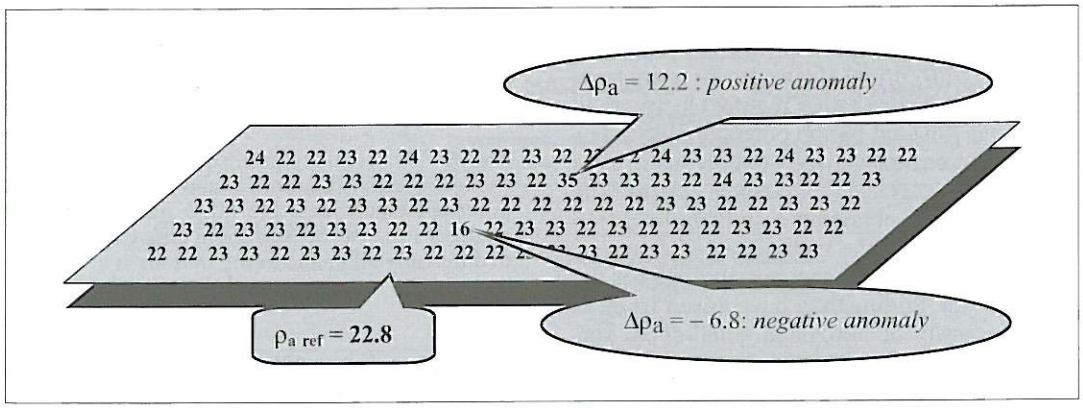

Fig. 5. Example of resistivity data collected on a grid. Reference resistivities as well as positive and negative resistivity anomalies are shown.

recalculated values to be back-projected $\rho_a[x, y]$ have to be analyzed before the back-projection and then:

– If the coefficient is positive (depending on τ and λ) they will be back-projected straightforwardly without any problem and the value to project $\rho_a[x, y]_{bp}$ will correspond to the measured datum $\rho_a[x, y]$.

– If the coefficient (particular values of τ and λ) is negative, then the value to project $\rho_a[x, y]_{bp}$ will be changed with respect to the measured datum $\rho_a[x, y]$ and it will become

$$\rho_a[x, y]_{bp} = \rho_{a_{ref}} - \Delta\rho_a[x, y] \qquad (3.4)$$

while the corresponding coefficient is taken as positive.

Thus this procedure allows us to use all the calculated coefficients, without problems of normalization, as the influence coefficients, useful to calculate the filter $g(\tau, \lambda, z)$, practically became all positive. The pseudo-inversion of the resistivity anomaly $\Delta\rho_a[x, y]$ can be also carried out following a finer procedure (Cosentino *et al.*, 1998b), but the differences between the results obtained using the two methods would be not very significant.

4. The resistivity grid: square and triangular mesh

Actually, the proposal of using a resistivity grid is quite old (rectangle method, see for instance, Kunetz, 1966). The method was used generally with current electrodes far away from the grid, to ensure a rather regular electric field in the area covered by the potential electrodes. The restitution was carried out only using field data, suitably corrected for boundary errors. The impossibility of obtaining a suitable inversion of field data made the method out of date.

In the last decade, new possibilities for the revival of the grid method have arisen from:

– Necessity of horizontal small-depth surveys for archaeological, environmental and engineering researches.

– Development of multi-channel geoelectrical instruments using multi-channel (both «intelligent» and «stupid») cables.

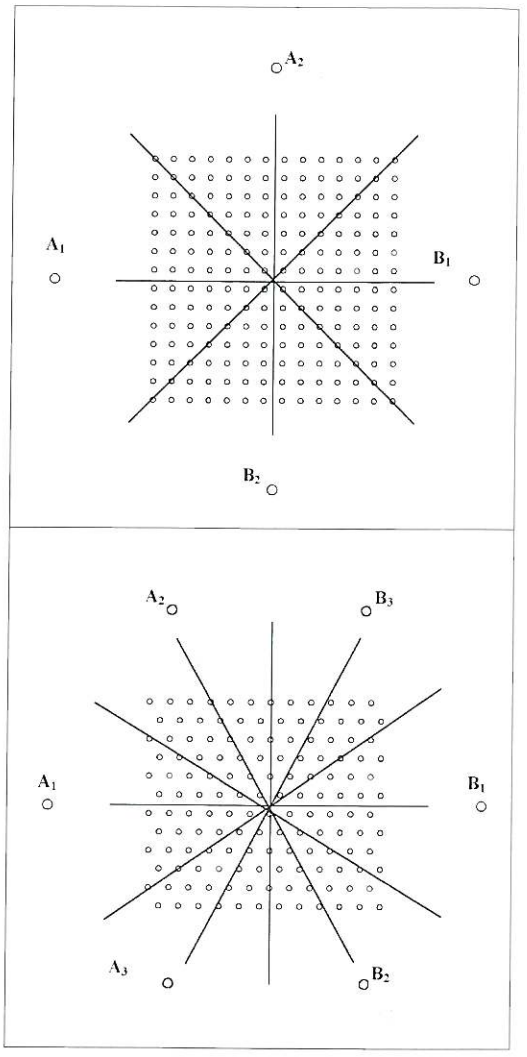

Fig. 6. The resistivity grid, square mesh (top) and triangular mesh (bottom). Small circles represent potential electrodes, the large one are current electrodes and can be oriented in different directions to differently «illuminate» the subsoil.

– Possibilities of 3D pseudo-inversion (back-projection tomography) of data and 2D inversion using both smooth and sharp boundary models (see, for instance, Loke and Barker, 1996).

– Possibility of using all the desired positions for the transmitter dipole (current electrodes) to illuminate the subsoil in various directions to recover the best result for the purpose of the investigation.

– Finally, the possibility of investigating new suitable parameters. For instance, the use of different azimuths for energy may also suggest using the resistivity tensor (Bibby, 1977; Bibby and Hohmann, 1993) to calculate a set of parameters which are invariant to rotation and then obtain a better and reliable recovery of the geometry of the buried structures.

Therefore, the rectangle method can be used once again (Cosentino *et al.*, 1999), both using rectangular and triangular arrangements of the potential electrodes (fig. 6), the choice being linked to practical and theoretical reasons. In fact, from a practical and technical point of view, the best way to measure the potential is along the same direction as the current lines and/or in a no orthogonal direction (so that it will be possible to calculate the apparent resistivity values). From theoretical problems, it is a good choice to arrange the voxel in the subsoil following the potential electrode array, so that the choice should be made on the basis of the assumed geometry of the possible anomalies in the subsoil. However, it is generally good practice to execute square grids using two (or four) directions of the current electrodes and triangular grids using three (or six) directions of the current electrodes (of course, to obtain a better resolution).

A suitable geoelectrical instrumentation, useful to carry out the measurements in a grid, can be arranged as shown in fig. 7. The main necessity is to use many simultaneous channels, so that a very fast multiplexing of 150-250 channels is useful to maintain exactly the same current, avoiding a source of errors. There is no need for «intelligent» cables and electrodes, as the current electrodes can be taken in a separate high-voltage cable. The whole apparatus, especially if characterized by high-impedance for the voltage-electrodes, then avoiding a long time to ensure appropriate resistance contacts, can be arranged for very fast measurements.

To summarize the steps of geoelectrical tomography, the following list can be proposed:

1) All the weights (sensitivities) have to be calculated for «distributing» each resistivity measure in the subsoil: the normalized weights are the *a priori* coefficients of the convolution process.

2) The set of experimental data is analyzed (modal analysis) to identify the reference resistivity (background resistivity). This resistivity value should correspond to the resistivity of the homogeneous soil, if any.

3) The resistivity of each voxel of the tomographic volume is then calculated by a convolu-

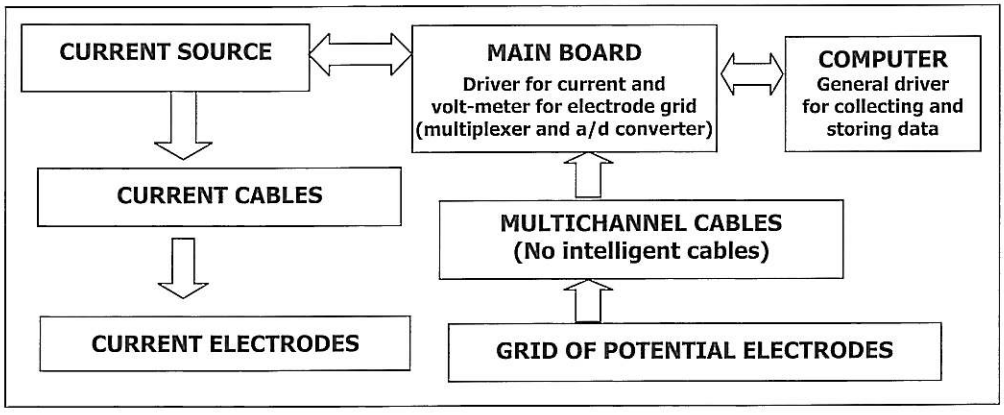

Fig. 7. Possible instrumentation for investigating the subsoil using the resistivity grid.

tion of all the experimental data with the normalized weights connecting the voxel with all data. During this process, when the weight is negative, the experimental datum is changed (the anomaly is inverted with respect to the reference value) and the weight is inverted to a positive value.

4) A first 3D tomographic matrix is obtained.

5) Finally some further processing can be made to improve the results. In fact, the weights can be corrected using a probabilistic approach and the back-projection can be repeated.

As to regards the last point, a filtering technique, useful for better detecting sharp boundary anomalies in the subsoil, is the following.

The back projection may be repeated using a new set of coefficients (some of them are put to zero, so that a re-normalization process is required): after the examination of the first tomographic rendering (with particular regard to the contained resistivity anomalies), the coefficients connecting the voxels with the experimental resistivity data are put to zero in the following cases:

– The tomographic resistivity of the voxel is higher than 80% of the maximum anomaly obtained in the back-projection and the connected experimental apparent resistivity value is lower than 80% of the maximum measured resistivity anomaly.

– The tomographic resistivity of the voxel is lower than 80% of the minimum anomaly obtained in the back-projection and the connected experimental apparent resistivity value is higher than 80% of the minimum measured resistivity anomaly.

– The tomographic resistivity of the voxel is lower than 80% of the maximum anomaly AND higher than 80% of the minimum anomaly in the back-projection and the connected experimental apparent resistivity anomaly is:

– OR higher than 80% of the maximum measured resistivity anomaly,

– OR lower than 80% of the minimum measured resistivity anomaly.

This technique can be slightly changed without large differences, depending on the supposed sharpness of the boundaries of the buried anomalies.

5. Some synthetic examples

The examples presented in figs. 8 to 13 refer to some synthetic models: the «experimental» data have been calculated simulating the application of the square grid and two current directions (namely those parallel to the edges of the square). This means that the integrated data take the advantage of two orthogonal directions for the illumination of the subsoil. It can be possible, however, to use more than two directions, and the results would be better and better.

The data were processed without any previous superposition of random errors. Nevertheless, some tests have been made using a perturbation of 5% random errors: the results seem do not significantly differ from those presented in the figures.

The various selected anomalies respectively are:

– a cubic (3×3×3 m) resistive body buried at a depth of 2 m (top) and 4 m (bottom) in the central part of the grid in fig. 8;

– a cubic (3×3×3 m) conductive body buried at a depth of 2 m (top) and 4 m (bottom) in the central part of the grid in fig. 9;

– a cubic (3×3×3 m) resistive (top) and conductive (bottom) body buried at a depth of 2 m in a not-centered part of the grid in fig. 10;

– two cubic (3×3×3 m) resistive and conductive body buried at a depth of 2 m in two different not-centered parts of the grid in fig. 11;

– a conductive pipe (2 m of diameter) buried at a depth of 0.5 m in the central part of the grid in fig. 12;

– an *L*-shaped resistive (top) and conductive (bottom) body buried at a depth of 0.5 m in the central part of the grid.

All the back-projections were repeated, after filtering of the coefficients as described in the previous chapter. All these figures are converted in black and white; only fig. 11 is still in color to be used as a guide for understanding the b/w ones.

Finally a very important problem regards the choice of both size and position of the voxels with respect to the anomaly model as well as the choice of both size and position of the voxels used to restore the obtained back-projection (using one of the recent programs, for instance

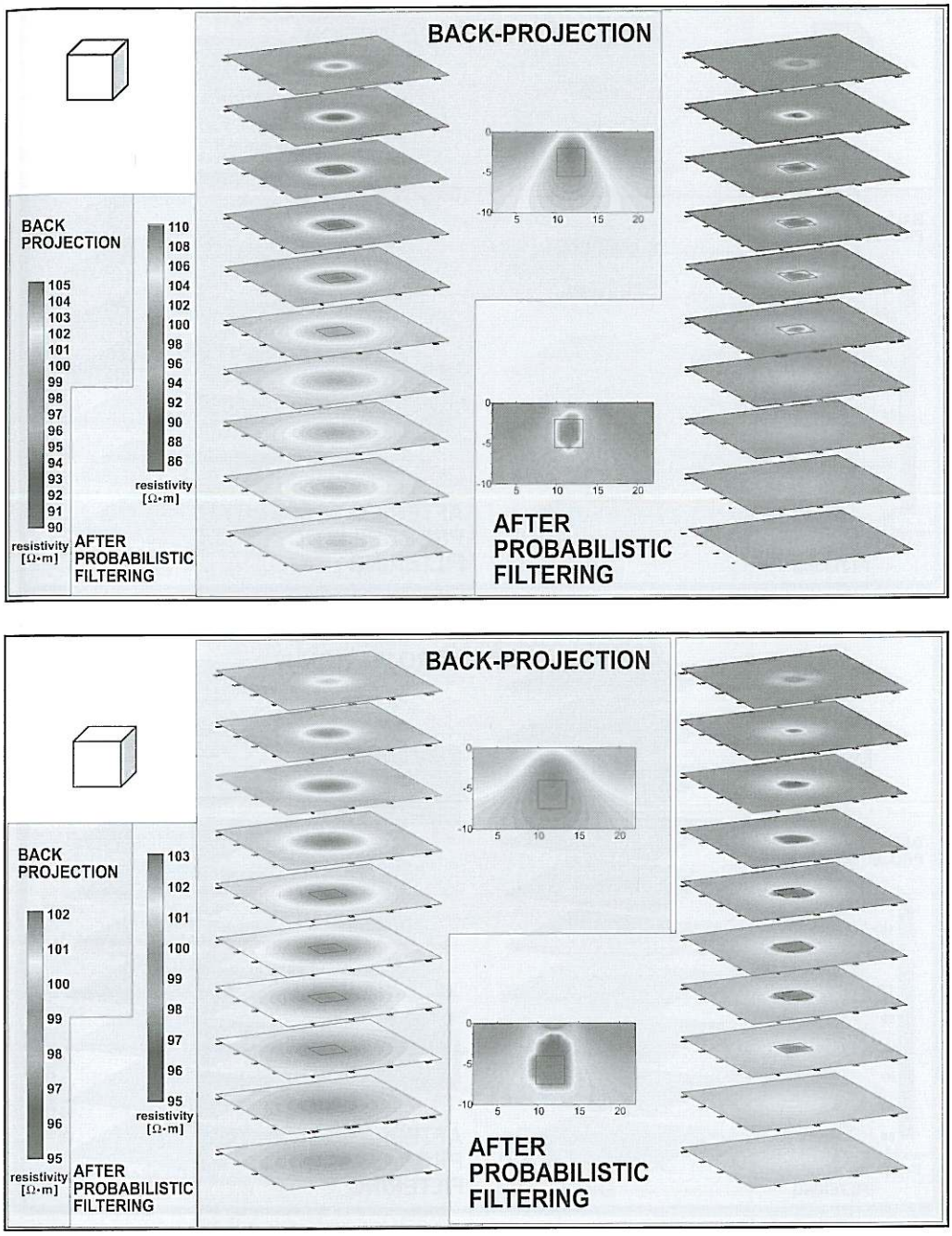

Fig. 8. Tomographic restitution of a cubic (3×3×3 m) resistive body buried at a depth of 2 m (top) and 4 m (bottom) in the central part of the grid. In both cases, the left restitution was obtained after the probabilistic filtering technique described in the paper.

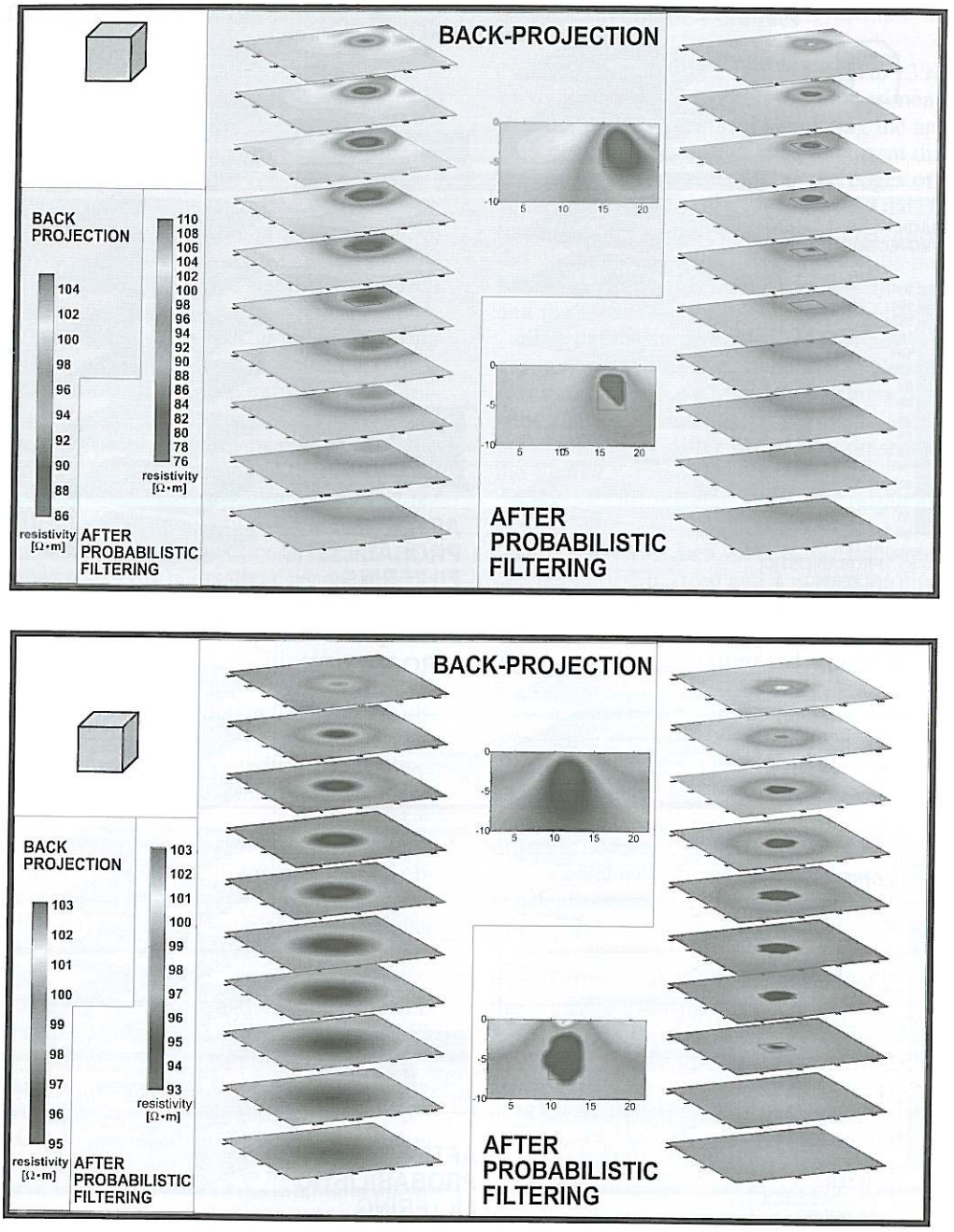

Fig. 9. Tomographic restitution of a cubic (3×3×3 m) conductive body buried at a depth of 2 m (top) and 4 m (bottom) in the central part of the grid. In both cases, the left restitution was obtained after the probabilistic filtering technique described in the paper.

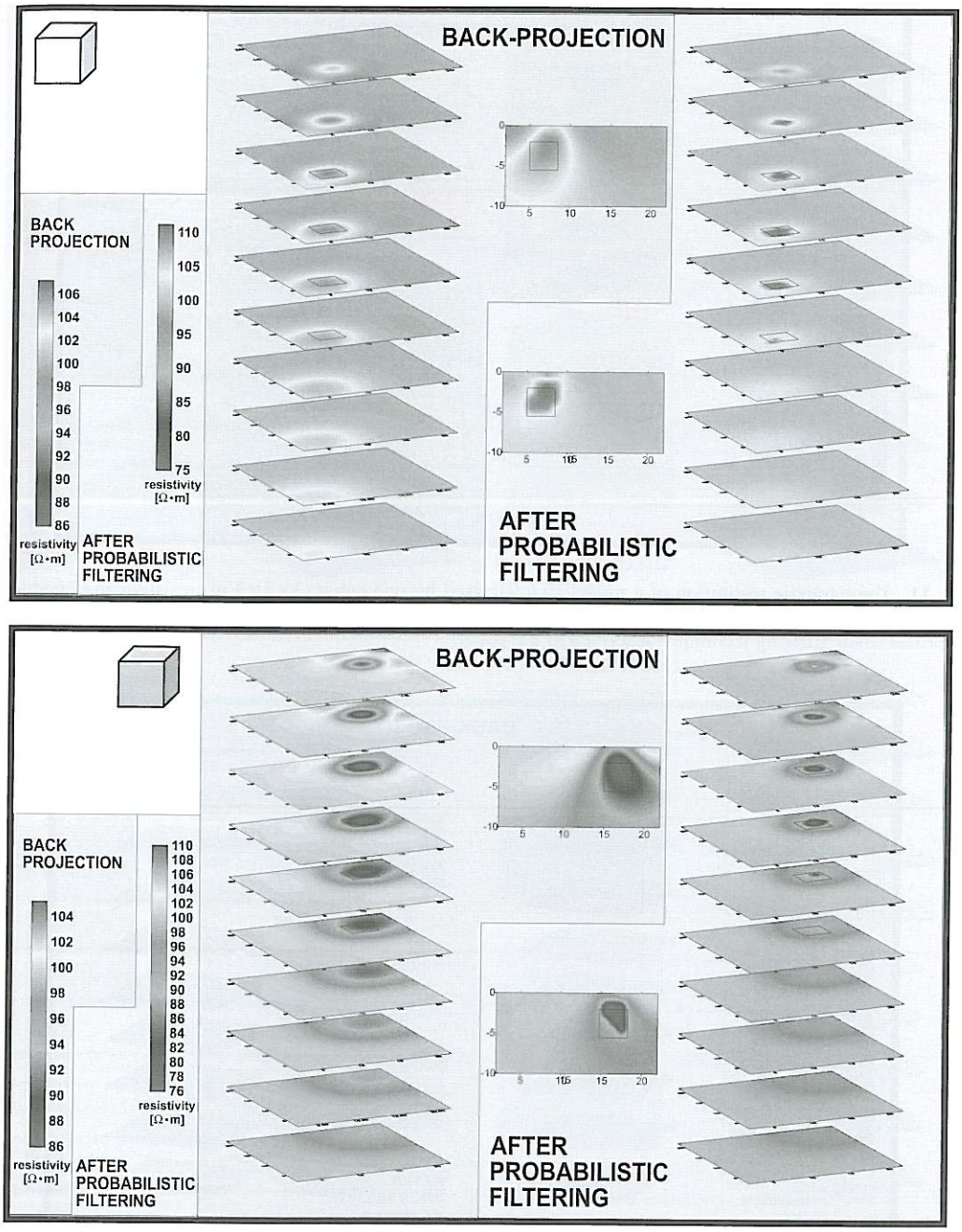

Fig. 10. Tomographic restitution of a cubic (3×3×3 m) resistive (top) and conductive (bottom) body buried at a depth of 2 m in a not-centered part of the grid. In both cases, the left restitution was obtained after the probabilistic filtering technique described in the paper.

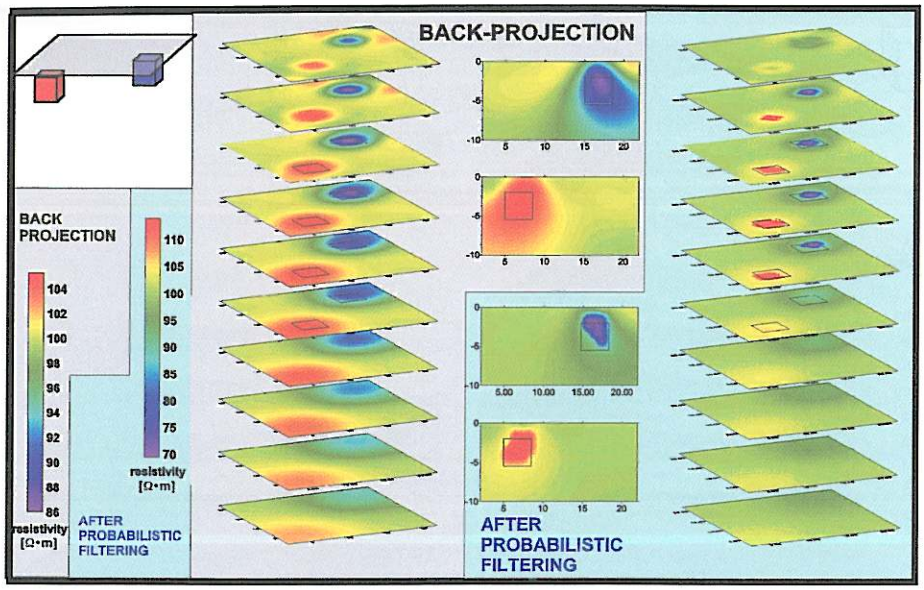

Fig. 11. Tomographic restitution of a model characterized by two cubic (3×3×3 m) resistive and conductive body buried at a depth of 2 m in two different not-centered parts of the grid. The left restitution was obtained after the probabilistic filtering technique described in the paper.

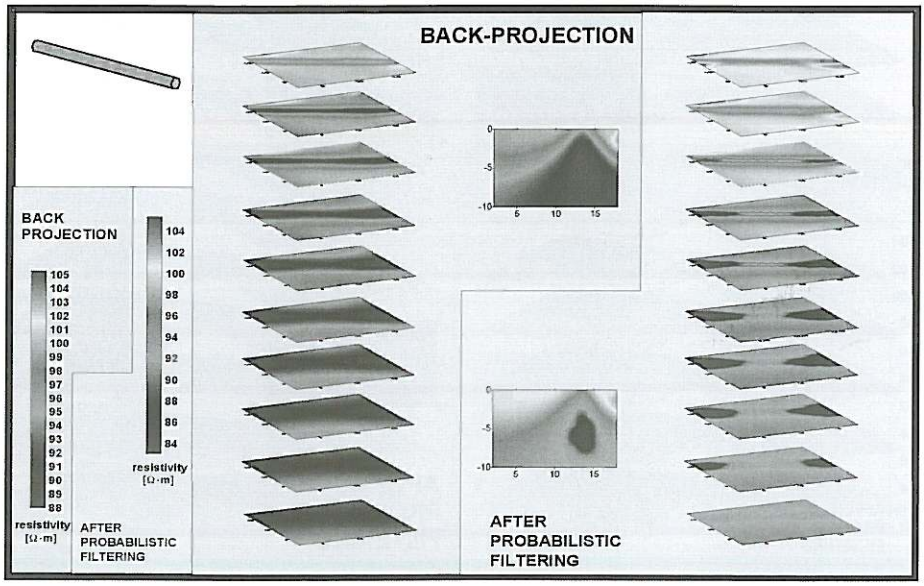

Fig. 12. Tomographic restitution of a model characterized by a conductive pipe (2 m of diameter) buried at a depth of 0.5 m in the central part of the grid. The left restitution was obtained after the probabilistic filtering technique described in the paper.

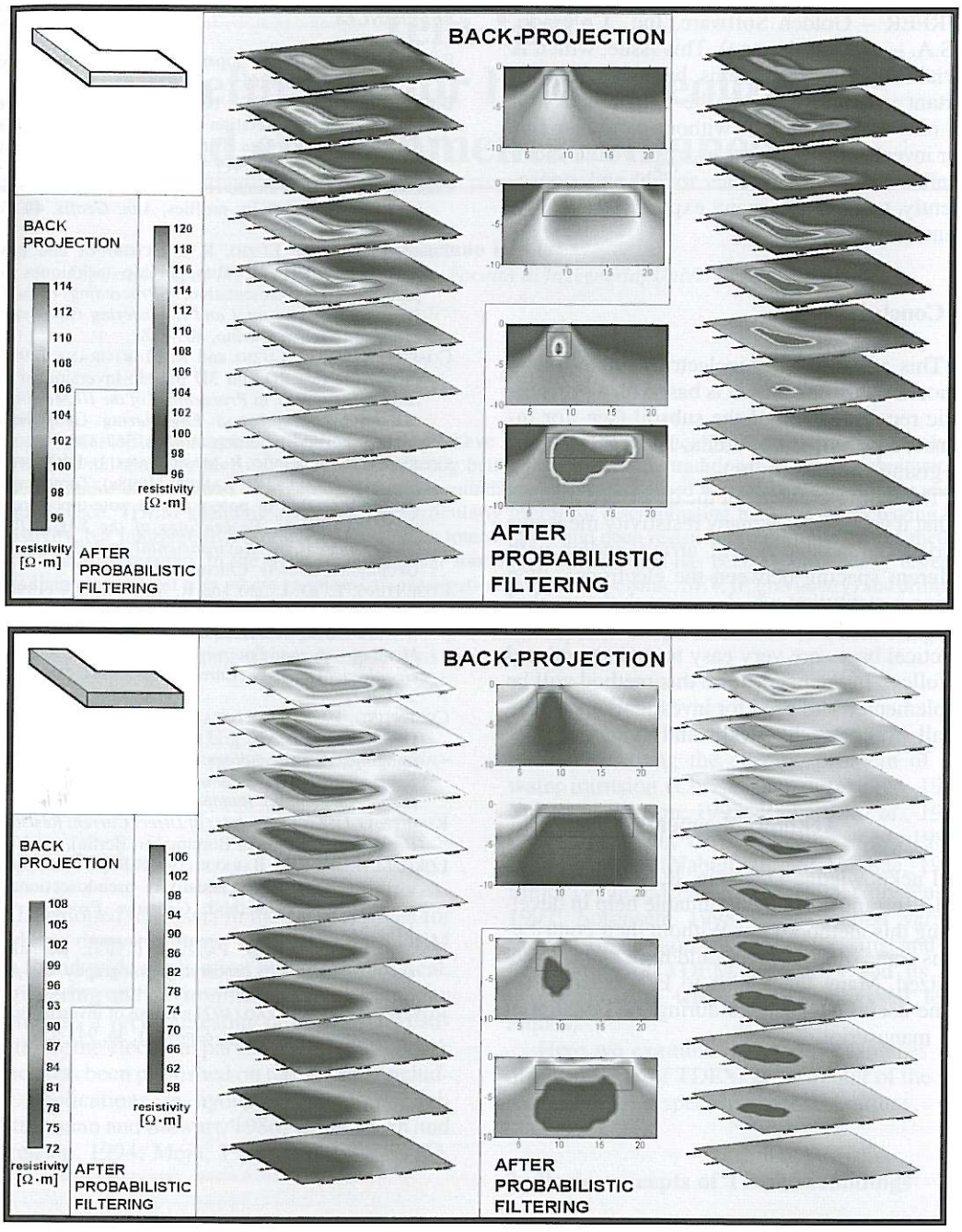

Fig. 13. Tomographic restitution of a model characterized by a *L*-shaped resistive (top) and conductive (bottom) body buried at a depth of 0.5 m in the central part of the grid. In both cases, the left restitution was obtained after the probabilistic filtering technique described in the paper.

SURFER – Golden Software, Inc., Colorado, U.S.A. – or a similar one). This issue, which is trivial in synthetic problems, becomes very important in the practice of the field researches: the only way to solve it without particular further investigation is to use a size of voxels much smaller than the anomalies sought and, consequently, to carry out many experimental measurements.

6. Conclusions

This approach to geoelectrical tomography is not the only one which is based on a probabilistic reconstruction of the subsoil (see, for instance, Mauriello and Patella, 1999, their method giving similar results).

The main advantage of the described method is that it can integrate many resistivity measures carried out with different arrays and/or with different spacing between the electrodes, then giving a restitution which can reach the level of detail needed. In addition, its theoretical and practical bases are very easy to understand and to follow. In the near future this method will be implemented and used for investigations also in small structures, like walls and monuments.

Acknowledgements

I acknowledge D. Luzio, R. Martorana and M.L. Terranova for their valuable help in developing this methodology. Without their contributions some of my work would have never materialized. Many thank also to E. Cardarelli for some useful suggestions during the revision of the manuscript.

REFERENCES

BIBBY, H.M. (1977): The apparent resistivity tensor, *Geophysics*, **42**, 1258-1261.

BIBBY, H.M. and G.W. HOHMANN (1993): Three-dimensional interpretation of multiple-source bipole-dipole resistivity data using the apparent resistivity tensor, *Geophys. Prospect.*, **41**, 697-723.

COSENTINO, P. and D. LUZIO (1997): Tomographic pseudo-inversion of resistivity profiles, *Ann. Geofis.* **40** (5), 1127-1144.

COSENTINO, P., D. LUZIO, R. MARTORANA and L.M. TERRANOVA (1995): Tomographic techniques for pseudo-section representation, in *Proceedings of the 1st Meeting Environmental and Engineering Geophysics, European Section, Torino*, 485-488.

COSENTINO, P., D. LUZIO and R. MARTORANA (1997): Filters for fast 2D and 3D pseudo-inversion of the resistivity profiles, in *Proceedings of the III Meeting of the Environmental and Engineering Geophysical Society, European Section, Aarhus*, 367-370.

COSENTINO, P., D. LUZIO, R. MARTORANA, L. D'ONOFRIO, M. MARCHISIO and G. RANIERI (1998a): Tomographic pseudo-inversion of pole-pole and pole-dipole resistivity profiles, in *Proceedings of the SAGEEP 98 Conference of the Environmental and Engineering Geophysical Society, Chicago*, 1009-1018.

COSENTINO, P., D. LUZIO and R. MARTORANA (1998b): Tomographic resistivity 3D mapping: filters coefficients and depth corrections, in *Proceedings of the IV Meeting of the Environmental and Engineering Geophysical Society (European Section), Barcelona*, 279-282.

COSENTINO, P., R. MARTORANA and L.M. TERRANOVA (1999): The resistivity grid to optimize tomographic 3D imaging, in *Proceedings of the V Meeting of the Environmental and Engineering Geophysical Society (European Section), Budapest*, Em 12, p. 2.

KUNETZ, G. (1966): *Principles of Direct Current Resistivity Prospecting* (Gebruder Borntraeger, Berlin), pp. 103.

LOKE, M.H. and R.D. BARKER (1996): Rapid least-square inversion of apparent resistivity pseudosections by a quasi-Newton method, *Geophys. Prospect.*, **44**, 131-152.

MAURIELLO, P. and D. PATELLA (1999): Resistivity anomaly imaging by probability tomography, *Geophys. Prospect.*, **47**, 411-429.

ROY, A. and A. APPARAO (1971): Depth of investigation in direct current methods, *Geophysics*, **36**, 943-959.